applied optics

Quantitative measurements of turbid liquids via structured laser illumination planar imaging where absorption spectrophotometry fails

Guy-Oscar Regnima,[1] Thomas Koffi,[1] Olivier Bagui,[1] Abaka Kouacou,[1] Elias Kristensson,[2] Jeremie Zoueu,[1] and Edouard Berrocal[2,*]

[1]Laboratoire d'Instrumentation, Image et Spectroscopie, (L2IS), INPHB, DFR-GEE, Yamoussoukro, Côte d'Ivoire
[2]Department of Physics, Division of Combustion Physics, Lund University, Lund, Sweden
*Corresponding author: edouard.berrocal@forbrf.lth.se

Received 27 February 2017; revised 5 April 2017; accepted 7 April 2017; posted 10 April 2017 (Doc. ID 287460); published 1 May 2017

A comparison between the commonly used absorption spectrophotometry and a more recent approach known as structured laser illumination planar imaging (SLIPI) is presented for the characterization of scattering and absorbing liquids. Water solutions of milk and coffee are, respectively, investigated for 10 different levels of turbidity. For the milk solutions, *scattering* is the dominant process, while the coffee solutions have a high level of *absorption*. Measurements of the extinction coefficient are performed at both $\lambda = 450$ nm and $\lambda = 638$ nm and the ratio of their values has been extracted. We show that the turbidity limit of valid transmission measurements is reached at an optical depth of OD ~ 2.4, corresponding here to an extinction coefficient of $\mu_e = 0.60$ mm^{-1} when using a modern absorption spectrometer having a spatial Fourier filter prior to detection. Above this value, errors are induced due to the contribution of scattered and multiply scattered photons reaching the detector. On the contrary, the SLIPI measurements were found to be very reliable, even for an extinction coefficient three times as high, where $\mu_e = 1.80$ mm^{-1}. This improvement is due to the capability of the technique in efficiently suppressing the contribution from multiple light scattering.

OCIS codes: (290.2200) Extinction; (290.4210) Multiple scattering; (290.7050) Turbid media; (300.0300) Spectroscopy; (300.1030) Absorption.

https://doi.org/10.1364/AO.56.003929

1. INTRODUCTION

There is a large variety of spectroscopy-based techniques that are intended for quantitative measurements in gaseous, solid, and liquid media. Among those, a popular approach is called *spectrophotometry* with many commercial instruments available on the market. One important feature of such instrumentation is its transmission measurement scheme, where the percentage of light crossing the probed volume can be measured at each wavelength of the visible spectrum. By extracting this quantity and using the Beer–Lambert–Bouguer law, the absorbance and the concentration of various compounds can be extracted. The technique is commonly used to determine the chemical component content in drugs [1], measure the value of iodine in vegetable oils [2], quantify the percentage of oxygen saturation and the amount of hemoglobin in very small blood samples [3], etc. While being very useful, these measurements are, unfortunately, no longer valid when applied to optically dense scattering media such as turbid liquids. This limitation is due to both the strong reduction of desired unscattered light and the large increase of unwanted scattered photons reaching the detector. The reduction of the desired signal can be compensated by using more sensitive sensors or brighter light sources. However, the effects of multiple light scattering are more challenging to account for. A few examples of optical approaches filtering the unscattered light are spatial Fourier filtering [4], polarization filtering [5], time gating [6], and structured illumination [7]. Recently, it has also been shown that the use of structured illumination together with Fourier filtering allows an efficient rejection of the multiply scattered light intensity resulting in transmission images of surprisingly high contrast [8].

Most often in spectrophotometry, the effects of multiple light scattering are reduced by simply using shorter paths through the scattering solution or by diluting the solution. While the smallest cuvettes are, for practical reasons, limited to a few millimeters, dilution is time consuming and can induce further errors in the measurements. As a result, optically dense media remain hard to probe using transmission measurements. For the case of highly turbid media, reflectance spectrophotometry is usually used [9,10]. However, the approach is not a direct measurement and relies on computational results using

the diffusion approximation or results from Monte Carlo simulation.

Another approach consists of detecting light from the side, perpendicular to the incident direction of propagation. One noticeable advantage of this source–detector configuration is the possibility of obtaining spatially resolved information, where the spatial resolution can be adjusted by varying the field of view of the camera. Therefore, the measurement is, in contrast to transmission, not restricted anymore by the fixed dimension of the cuvette containing the probed medium. However, one drawback is that filtering schemes, to reject the multiple light scattering, are hard to find. To the best of the authors' knowledge, the most efficient approach to suppress the light intensity contribution from multiple scattering on side detection is to use structured illumination on a laser sheet imaging scheme: a technique known as structured laser illumination planar imaging (SLIPI) [11]. This optical technique was first developed for the characterization of atomizing sprays. In such systems, a large amount of micrometric scattering droplets are generated, making the medium turbid and difficult to image. In addition to sprays, the technique has also been used to probe uniform solid–liquid dispersions [12] and to measure temperature in liquids [13]. Depending on the application, the technique has been used in various configurations consisting of three-phase [11], two-phase [14] and single-phase recordings [15]. The number of phases corresponds to the number of subimages that are recorded and processed to reconstruct the final SLIPI image. In this paper, the single-phase SLIPI approach used in Ref. [16] is employed to measure the extinction coefficient in different coffee and milk solutions. Two wavelengths, $\lambda = 450$ nm and $\lambda = 638$ nm, have been, respectively, used for 10 different solutions, which have been prepared at various dilution ratios. The SLIPI results are compared for the same wavelengths with the results obtained from transmission measurements using a commercial absorption spectrophotometer. The limits of classical absorption spectroscopy are highlighted in this paper and the possibility, with SLIPI, of obtaining reliable measurements in optically dense scattering liquids is demonstrated.

2. ABSORPTION SPECTROPHOTOMETRY

A. Measurement Principle and Limitations

Absorption spectrophotometry is an optical technique primarily used for analyzing the light absorption properties of a liquid solution containing various molecules. By deducing this light absorption as a function of wavelength, various substances can be distinguished one to another. The solution of interest is usually contained in a cuvette, where a collimated beam is crossing it along its width L. The light transmission through the sample is then measured at various desired wavelengths, which range in the ultraviolet and visible spectral regions for most standard spectrometers. Note though that modern detectors are now capable of increasing this range to the near-infrared region. In addition to the spectral absorption response of the probed substances, one common application is to deduce the concentration of the solutes contained within the solvent (e.g., water, ethanol, and acetone). The measurement can be described as follows.

First, the transmitted light I_0 is recorded using a "blank" reference cuvette containing only the solvent. Then, the transmitted light I_t is recorded, where both the solvent and the solutes are mixed. Thus, the absorption of the solute only can be quantified by taking the ratio between the two measurements. This corresponds to the transmittance T, which is a measure of the light attenuation along the distance L. According to the Beer–Lambert–Bouguer law and assuming a collimated beam of a single wavelength crossing a uniform medium, the transmittance T is given by

$$T = I_t/I_0 = e^{-\mu_e \cdot L} = e^{-\mathrm{OD}}, \tag{1}$$

where μ_e is the extinction coefficient and OD is the so-called optical depth. The extinction coefficient is related to the concentration N of molecules/particles contained within the solution as

$$\mu_e = N \cdot (\sigma_a + \sigma_s). \tag{2}$$

Here, σ_a and σ_s are the absorption and scattering cross sections, respectively. Using Eq. (1), μ_e is extracted as

$$\mu_e = -\ln(T)/L. \tag{3}$$

One key point for obtaining accurate transmission measurements is to have a scattering cross section as small as possible in comparison to the absorption cross section. Therefore, purely absorbing media are recommended in absorption spectrophotometry. However, purely scattering media lead to errors due to the detection of undesired scattered and multiply scattered light, as illustrated in Fig. 1. When a scattering medium is probed, it is recommended to dilute the solution or reduce L, such that only one scattering event or less occurs along the path through the medium.

The average distance $\overline{l_{\mathrm{fp}}}$ a photon travels between interactions with the solute molecules (or particles) is called the mean-free path length and can be deduced in a uniform medium from the inverse of the extinction coefficient:

$$\overline{l_{\mathrm{fp}}} = 1/\mu_e. \tag{4}$$

As a result, the optical depth OD corresponds to the average number of scattering and/or absorption events along the distance L as

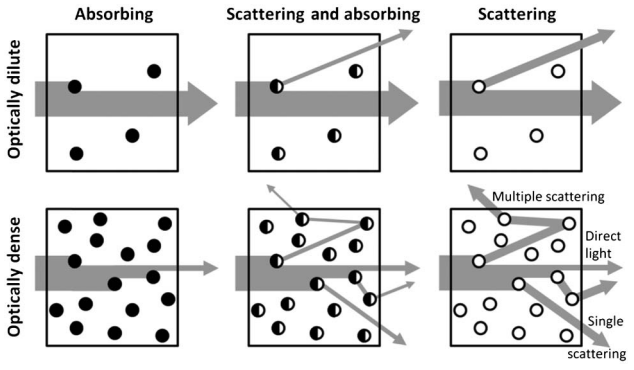

Fig. 1. Classification of absorbing and scattering media. For transmission measurements (e.g., absorption spectrophotometry), the optimum situation is to probe an optically dilute absorbing solution. However, an optically dense scattering medium will be very challenging to probe as undesired scattered light will be detected.

$$\mathrm{OD} = L/\overline{l_{\mathrm{fp}}}. \tag{5}$$

If the optical depth is smaller than one, OD ≤ 1, then the single scattering regime is assumed. If the optical depth is OD ≥ 10, then the diffusion approximation applies. For most turbid liquids, the resulting optical depth range is $2 \leq \mathrm{OD} \leq 9$, corresponding to the intermediate scattering regime [17]. In such cases, transmission measurements are most often erroneous.

Finally, the last quantity of importance, which is often used in chemistry, is the so-called absorbance A, which is related to the optical depth as

$$A = \mathrm{OD}/\ln(10) = -\log_{10} T. \tag{6}$$

An absorbance of one corresponds to 10% of light transmittance, while an absorbance of two corresponds to only 0.1% transmittance. Therefore, A gives a quick indication of how much of the light has crossed the sample, while the optical depth gives an indication of how many scattering or absorption events has occurred within the probed sample. Note that all the previous definitions are wavelength dependent. Thus, by using a collimated white source of light at the entrance of the cuvette and a spectrometer prior to detection, the absorbance can be spectrally resolved. Therefore, absorption spectrophotometry offers the possibility of providing simultaneous transmission measurements for each individual wavelength.

B. Optical Setup and Measurement Description

The absorbance spectra were acquired by using an optical spectrometry kit from Ocean Optics. The system is built-up from a USB4000-FL spectrometer, a white LED light source, two optical fibers, and a CUV-ALL-UV cuvette holder. A detailed schematic of the experimental arrangement is shown in Fig. 2. The white light source is guided to the cuvette holder using the first optical fiber. The cuvette holder is equipped with two identical spherical lenses of 5 mm diameter and $f = +10$ mm focal length, which are located on both sides of the cuvette. The first one is used for collimating the light exiting the first optical fiber, and the second one is used for focusing the remaining transmitted collimated light into the second optical fiber.

The transmitted light is then guided into the USB4000-FL spectrometer for spectral analysis. Light enters the spectrometer through a 200 μm slit and hits a collimating mirror that reflects the light into a grating of 3600 l/mm, which is set for the spectral range 360–1100 nm. The dispersed beam is then reflected by a mirror that focuses it onto a linear CCD array. According to the manufacturers, this detector has a maximum signal-to-noise ratio of 300:1. Thus, the maximum absorbance that can be measured is $A = 2.5$, which is equivalent to an optical depth of OD $= 5.7$.

The background is acquired when the light is off and subtracted from each recorded spectra. The reference signal I_0, which corresponds to the light intensity as a function of wavelength (see Fig. 3), is recorded from a cuvette containing only the solvent, which is water in this study. Then the signal I_t corresponding to the transmitted spectrum of both the solvent and the solute is recorded. By finally dividing those two signals, the transmittance for each wavelength is obtained and the spectral absorbance can be derived using Eq. (6). A cuvette of short length, where $L = 4$ mm (instead of the common distance

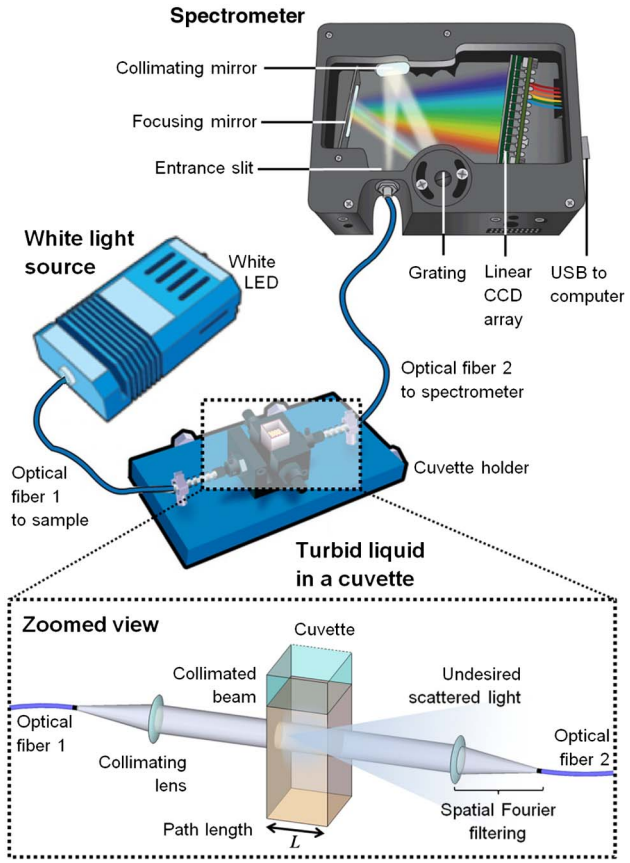

Fig. 2. Illustration adapted from Ocean Optics of the absorption spectrophotometer. A zoomed view of the optical arrangement around the cuvette is also given. White light exits the first optical fiber at the focus of a collimating lens. The collimated white beam crosses the turbid solution and is collected using another lens, focusing it into a second optical fiber. This light is then spectrally dispersed and analyzed using the USB4000-FL spectrometer from Ocean Optics.

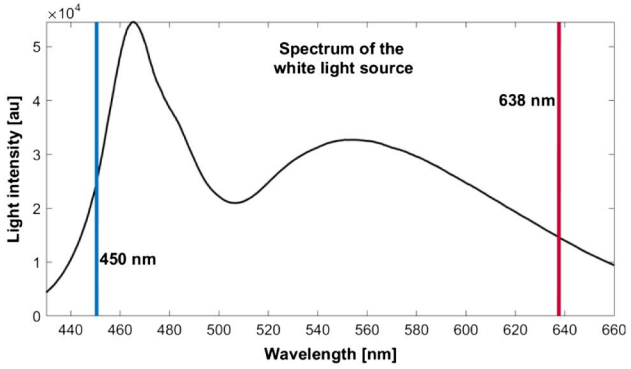

Fig. 3. Spectrum of the white LED light used in the experiment. This spectrum has been recorded with 40 ms exposure time and serves as the reference. The 450 nm and 638 nm wavelengths corresponding to the SLIPI illumination wavelengths are indicated on the spectrum.

10 mm), has been used here in order to probe solutions of higher concentration. Using this length and the transmittance, the extinction coefficient is extracted at 450 nm and 638 nm wavelengths using Eq. (3).

3. SINGLE-PHASE SLIPI

A. Measurement Principle

The single-phase SLIPI approach used in the current study is based on an analytical tool known as lock-in detection [18]. Lock-in detection is most often associated with analysis of *temporally* varying signals, but it works equally well for *spatially* modulated signals. To explain the principle of lock-in detection, consider a 1D signal, $I(x)$, with a superimposed periodic variation of amplitude I_S in space:

$$I(x) = I_S \sin(2\pi\nu x + \phi) + I_{\mathrm{MS}}(x), \quad (7)$$

where ν equals the spatial frequency (mm^{-1}) of the modulation and ϕ is the spatial phase, which is unknown. The I_{MS} term represents any unwanted nonmodulated intensity contribution also being detected, such as multiple light scattering or any surrounding light background. The purpose of the lock-in analysis is to extract I_S and reject I_{MS}. To achieve this end, the signal I is multiplied with two reference signals R_1 and R_2, created computationally, that have a relative phase shift of $\pi/2$:

$$R_1(x) = \sin(2\pi\nu x) \quad \text{and} \quad R_2(x) = \cos(2\pi\nu x). \quad (8)$$

Multiplying I with these reference signals yields

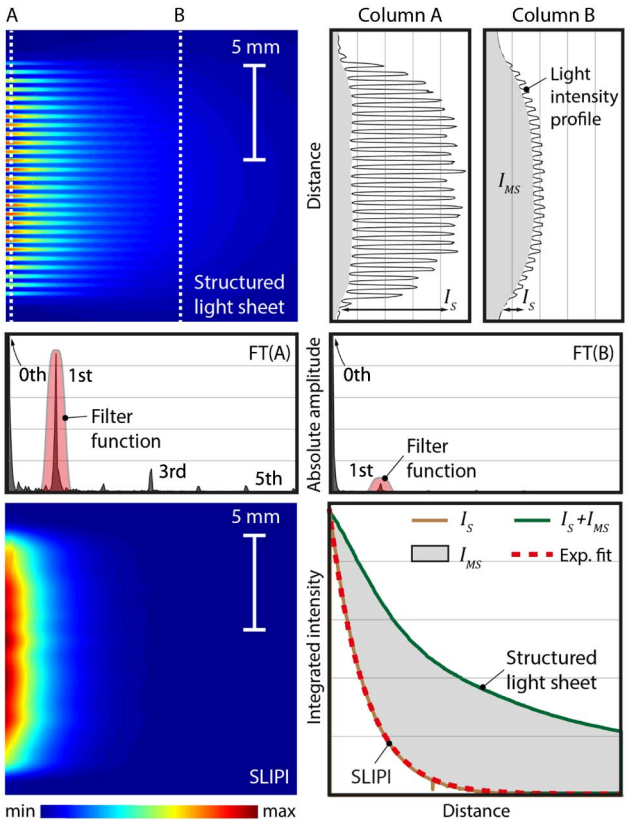

Fig. 4. Principle of single-phase SLIPI. The example shows the signal from a structured laser sheet with cross sections extracted from two different depths, marked as A and B. Notice the decrease in amplitude from column A to B. The 1D Fourier transforms of curves A and B show the reduction in strength of the first-order peak (modulation frequency). This frequency is then isolated using frequency filtering (red area) after applying the lock-in algorithm. Finally, the exponential decay is revealed, as shown in the SLIPI image and related curve I_S.

$$I_1(x) = \frac{1}{2} I_S(\cos(\phi) - \cos(4\pi\nu x + \phi)) + I_{\mathrm{MS}} \sin(2\pi\nu x), \quad (9)$$

$$I_2(x) = \frac{1}{2} I_S(\sin(\phi) + \sin(4\pi\nu x + \phi)) + I_{\mathrm{MS}} \cos(2\pi\nu x). \quad (10)$$

The frequency analysis of I_1 and I_2 reveals three components: (1) a DC component, (2) one modulated with 2ν, and (3) one modulaed with ν. The two latter components can be suppressed by means of a low-pass filter in the Fourier domain, with a cutoff frequency less than ν, resulting in the following expressions:

$$\widetilde{I}_1(x) = \frac{1}{2}\widetilde{I}_S \cos(\phi) \quad \text{and} \quad \widetilde{I}_2(x) = \frac{1}{2}\widetilde{I}_S \sin(\phi), \quad (11)$$

where the tilde assignment indicates the applied frequency filtering. From these, $\widetilde{I}_S$ can finally be extracted by calculating

$$\widetilde{I}_S = 2\sqrt{(\widetilde{I}_1)^2 + (\widetilde{I}_2)^2}. \quad (12)$$

An illustration of the single-phase SLIPI process is given in Fig. 4. From a modulated image, the amplitude of the modulation is extracted using Eq. (12). The modulated component, I_S, corresponds to the single light scattering, which reduces exponentially with distance. By applying an exponential fit to I_S, the extinction coefficient, μ_e, can be directly extracted as stated in the Beer–Lambert–Bouguer law [see Eq. (1)].

B. Optical Setup and Measurements

The light sources consist of two continuous-wave (CW) laser beams of 450 nm and 638 nm, which are recombined along the same optical path using a dichroic mirror. One laser is activated at a time and a neutral density wheel is used to adjust the incident irradiance in order to optimize the signal-to-noise ratio while avoiding saturation. The beam is then expanded by a factor of × 10 using a telescope arrangement made of a pair of positive spherical lenses. An aperture is used to select the central part of the beam where the spatial intensity profile is fairly homogeneous. A positive cylindrical lens of a 200 mm focal lens is used to create the light sheet into the cuvette. To spatially modulate this light sheet, a Ronchi grating of 2 lp/mm is directly fixed onto a cuvette of 20 mm width. Thus, perfect modulation is created just at the entrance of the cuvette, limiting unwanted effects caused by near-field diffractions known as the Talbot effect [19]. In order to reduce signal attenuation as light propagates from the structured light sheet toward the camera, the location of the illumination plane is fixed as close as possible from the cuvette glass wall (~2 mm) facing the camera. The images are recorded using a 14 bit electron-multiplying- (EM) CCD camera, Luca (r) from Andor, and the final image is the result of the accumulation over 200 single-shot images. The camera objective is set to $F\# = 5.6$, and the exposure time ranges between 0.001 and 0.01 s to optimize the dynamic range for each concentration cases. The more diluted solutions were generating a lower signal than the more concentrated ones, having, therefore, longer exposure times. A detailed schematic of the optical setup is given in Fig. 5.

4. METHODOGY AND RESULTS

A. Preparation of the Participating Solutions

The milk solutions are prepared using evaporated milk (from the brand “Bonnet Rouge”) characterized by more than 9% fat

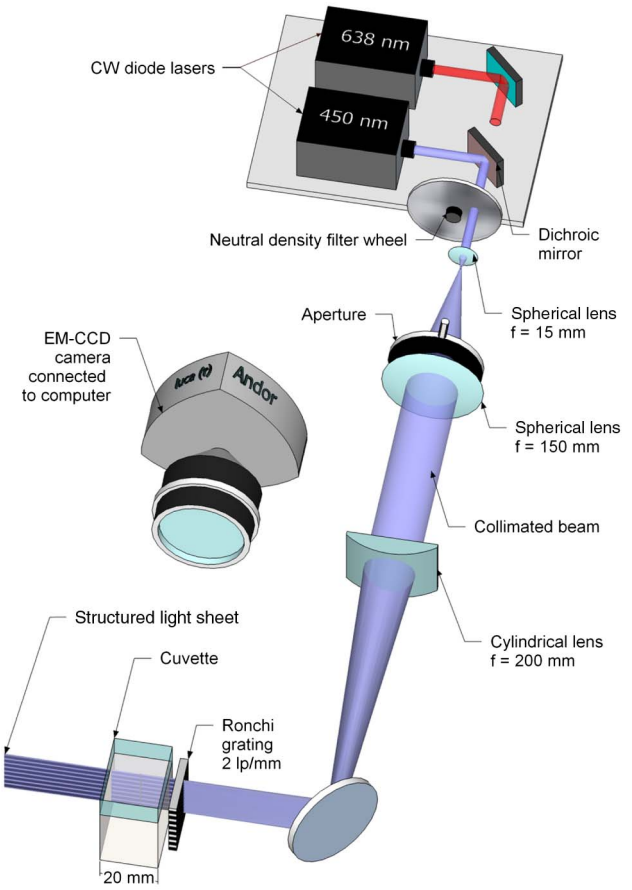

Fig. 5. SLIPI optical setup. After expanding the incident laser beam, a light sheet is formed by using a cylindrical lens focusing the beam into the cuvette. The light sheet is modulated just prior to entering the cuvette containing the turbid liquid by a Ronchi grating of 2 lp/mm frequency. The images are recorded using an EM-CCD camera.

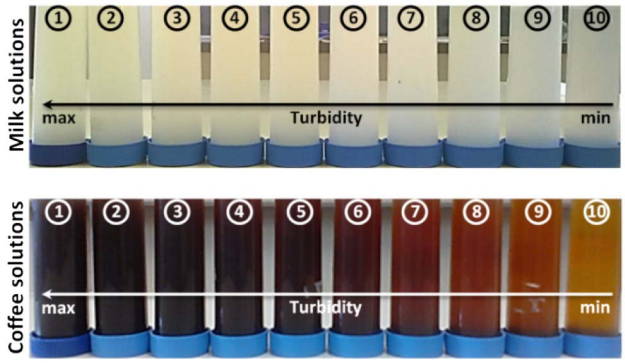

Solution	Milk dilutions	Coffee dilutions	C
①	V_1 = 5ml milk + 495 ml water	V_1 = 6 g coffee + 450 ml water	1.0 x C_1
②	V_2 = 67.5 ml V_1 + 7.5 ml water	V_2 = 67.5 ml V_1 + 7.5 ml water	0.9 x C_1
③	V_3 = 60.0 ml V_1 + 15.0 ml water	V_3 = 60.0 ml V_1 + 15.0 ml water	0.8 x C_1
④	V_4 = 52.5 ml V_1 + 22.5 ml water	V_4 = 52.5 ml V_1 + 22.5 ml water	0.7 x C_1
⑤	V_5 = 45.0 ml V_1 + 30.0 ml water	V_5 = 45.0 ml V_1 + 30.0 ml water	0.6 x C_1
⑥	V_6 = 37.5 ml V_1 + 37.5 ml water	V_6 = 37.5 ml V_1 + 37.5 ml water	0.5 x C_1
⑦	V_7 = 30.0 ml V_1 + 45.0 ml water	V_7 = 30.0 ml V_1 + 45.0 ml water	0.4 x C_1
⑧	V_8 = 22.5 ml V_1 + 52.5 ml water	V_8 = 22.5 ml V_1 + 52.5 ml water	0.3 x C_1
⑨	V_9 = 15.0 ml V_1 + 60.0 ml water	V_9 = 15.0 ml V_1 + 60.0 ml water	0.2 x C_1
⑩	V_{10} = 7.5 ml V_1 + 67.5 ml water	V_{10} = 7.5 ml V_1 + 67.5 ml water	0.1 x C_1

Fig. 6. Photographs of the samples prepared at various dilution ratios for the milk and the coffee. The increase in turbidity from right to left is apparent, especially in the case of the coffee solutions. The corresponding dilution procedure of each solution is provided in the table.

content. An initial solution C_1 is created by diluting 5 ml of milk within 495 ml of water. This dilution results in a concentration equal to 1% from the initial milk concentration C_0. Based on this first dilution, nine others solutions have been prepared to obtain a linear decrease in milk concentration. A detailed description of this dilution procedure is given in the table in Fig. 6.

The coffee solutions are prepared using instant coffee (from the brand "Nescafé Classic") made of 100% robusta coffee. An initial solution C_1 is created by dissolving 6 g of coffee into 450 ml of water. From this solution, nine solutions have been, once again, prepared to obtain a linear decrease in concentration, in a similar fashion that for the milk solutions.

The resulting 20 solutions are shown in Fig. 6. At high concentrations, the coffee appears black due to the important absorption from the coffee molecules. This is particularly true for the blue and green spectral regions. However, at low concentrations, the coffee solutions appear "yellowish–reddish," indicating that scattering is not negligible and also occurs in this spectral range. For milk solutions, its white color indicates that scattering is highly dominant in comparison to absorption through the entire visible wavelength range. Milk is a very complex food consisting of an emulsion of fat globules in suspension in a water solute. The size of the fat globules is larger than the wavelength and ranges around 2 μm in diameter [20]. As a result, when light interact with such particles, the angular distribution of the scattered radiation is governed by the Lorenz–Mie theory. In such cases, light does not scatter equally in all directions but mostly in the forward direction. This differs from the coffee solutions, where light is interacting with molecules of size much smaller than that of the incident wavelength, resulting in a Rayleigh scattering process.

B. Absorption Spectrophotometry Results

The absorbance spectra of the milk and coffee solutions are given in Figs. 7(a) and 7(b), respectively. In both cases, it is seen that the absorbance is more important in the blue spectral region than in the red spectral region. However, for the case of coffee, this difference is more pronounced than for milk. It is observed that for the highly concentrated solutions, the absorbance spectra become noisy due to low signal-to-noise ratios. This is particularly visible for wavelengths in the range of 440 nm. It can be explained such that the irradiance of the nonscattered light transiting the cell reduces exponentially with concentration. In addition, low light intensity detection around 440 nm is observed in Fig. 3 due to the combination of low light emission and low sensor sensitivity in this spectral region. As a result, the strong decrease in absorbance observed in the blue spectral region should not be interpreted as a characteristic of the probed media but as an undesired artifact due to a low signal-to-noise ratio. However, for the most diluted solutions, those effects are not visible and the recorded spectra are reliable. The spectral lines at 450 nm and 638 nm are also indicated on the graphs. Based

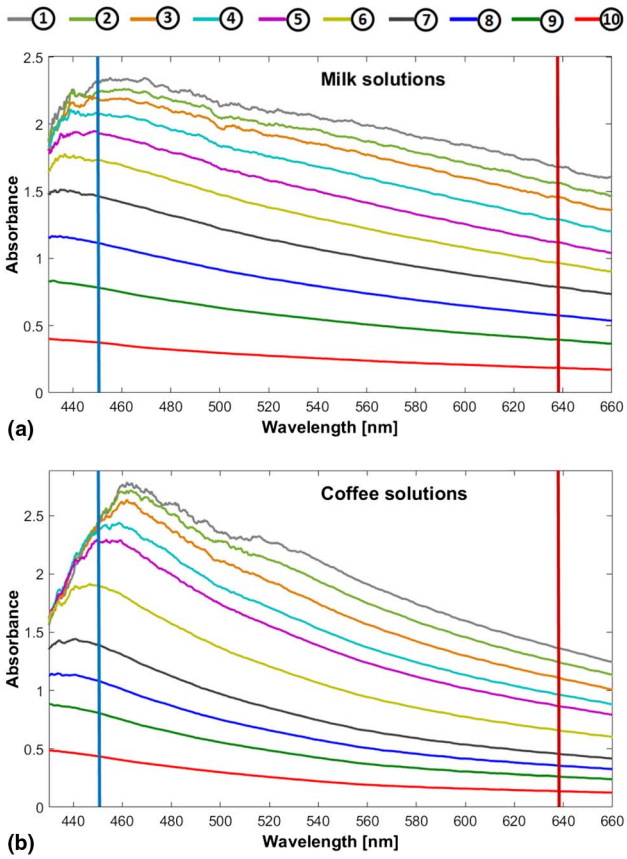

Fig. 7. Absorbance spectra of the milk solutions in (a) and the coffee solutions in (b) measured using absorption spectrophotometry. The increase of the absorbance with concentration is clearly seen. It can also be observed that the absorbance gives an equal value at high concentration and for the "blue" wavelength range due to too low of a signal-to-noise ratio in these conditions.

on the absorbance value at those wavelengths, the extinction coefficient is deduced by combining Eqs. (1) and (6) as

$$\mu_e = A \cdot \ln(10)/L, \tag{13}$$

where L is equal to 4 mm, corresponding to the length of the cuvette used in the spectrophotometry measurements.

C. Single-Phase SLIPI Results

The image results from the single-phase SLIPI measurements for the milk and coffee solutions are shown in Figs. 8 and 9, respectively. The dilution cases from ⑤ to ⑩ are shown here at 638 nm illumination wavelength. The image column on the left-hand side corresponds to the recorded raw images. It is seen from those images that the structured pattern enters the 20 mm width cuvette, from the left-hand side, and that this line structure disappears with distance as light propagates further through the cuvette. While at low concentration, the lines remain visible through the entire length of the cuvette and only become observable at the cuvette entrance at high concentration when the solutions are more turbid. In addition, it is seen from the milk solutions that a surrounding light background blurs the images. This light intensity originates from photons that have been scattered multiple times within the solution,

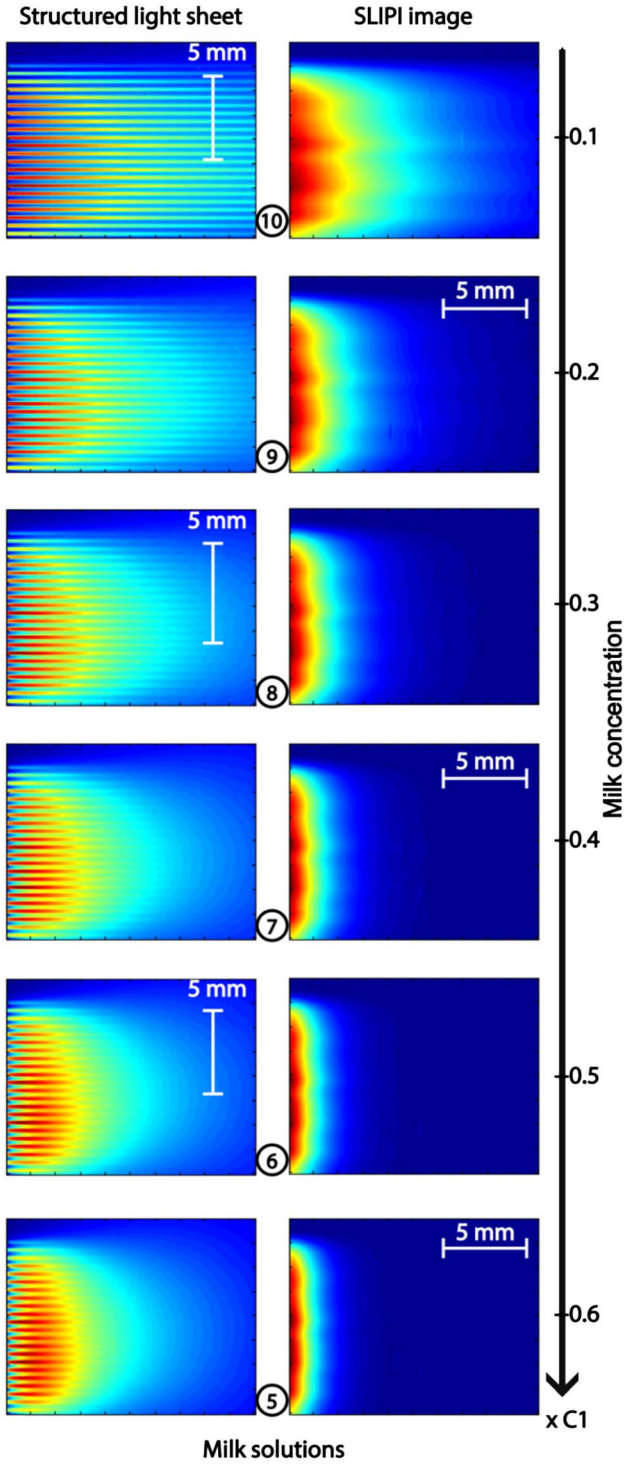

Fig. 8. Images of the structured light sheet crossing the cuvette at increased milk concentration. The corresponding SLIPI images are given on the right-hand side. As milk highly scatters light, blurring effects due to multiple light scattering are apparent on the modulated images. By suppressing this unwanted contribution and demodulating the signal, the SLIPI images are obtained, where the light extinction through the cuvette is clearly visible. By analyzing those images and fitting an exponential decay, the extinction coefficient can be directly deduced.

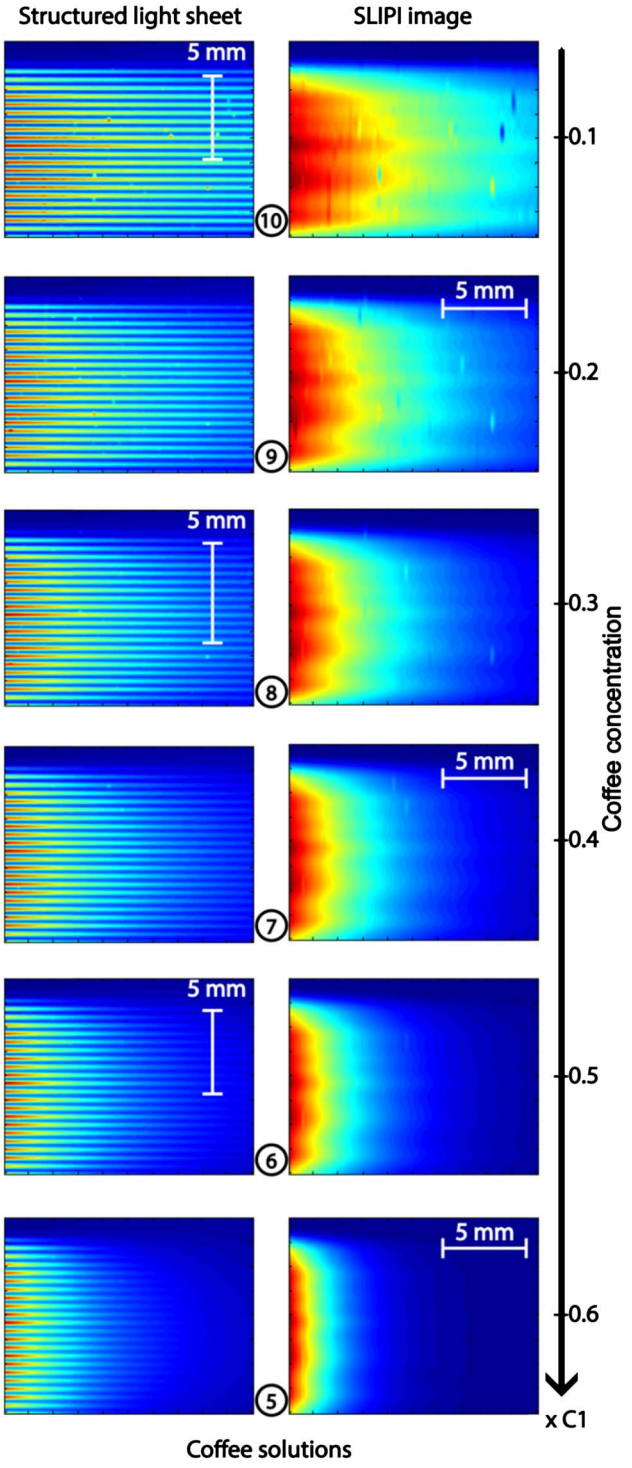

Fig. 9. Images of the structured light sheet crossing the cuvette at increased coffee concentrations. The corresponding SLIPI images are given on the right-hand side. As coffee is mostly absorbing, the blurring effects due to multiple scattering are less apparent here than for the milk case. However, there is still some remaining undesired scattered light that must be suppressed using SLIPI. Thus, the resulting SLIPI images depict the correct light extinction, where an exponential fitting of the intensity decay provides the corresponding extinction coefficient.

prior to detection. This effect is due to the nonabsorbing property of milk. Thus, at each interaction between light and the milk fat globules, photons are scattered and redirected away from the incident direction with nearly no loss in energy.

When now absorption is relevant, as in the case for the coffee solutions, the contribution of this surrounding light is strongly reduced. Thus, the absorption process, which occurs at each interaction between light and the coffee molecules, allows a better visualization of the line structure while at the same time reduces the total amount of light being detected by the camera. These effects of scattering and absorption can be seen when comparing the structured images between Figs. 8 and 9.

Note that the increasing of visibility in turbid media by means of absorption is not novel and has been reported by Alfano's group back in the 1990s [21].

By postprocessing the structured images and extracting the amplitude of the modulated structure, the SLIPI images are obtained as shown on the right-hand side of Figs. 8 and 9. In this case, the light intensity from multiple light scattering is efficiently removed and the surrounding blurs are not observable anymore, even for the cases of concentrated milk solutions. Those images reveal the intensity profile of the incident light sheet along the vertical direction, while having strong light intensity decay along the horizontal direction. When now vertically integrating the light signal from each SLIPI image, a curve of those decays is obtained.

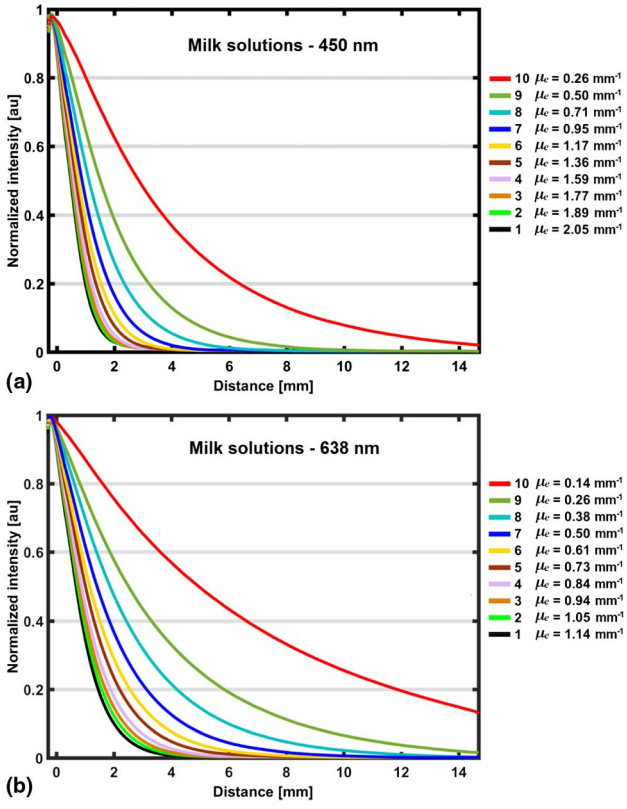

Fig. 10. Curves obtained by vertically integrating the SLIPI image results of the milk solutions for 450 nm illumination wavelength in (a) and 638 nm in (b). The exponential decay of the light intensity as a function of distance through the cuvette is obtained here, and the extinction coefficient has been deduced from those decays.

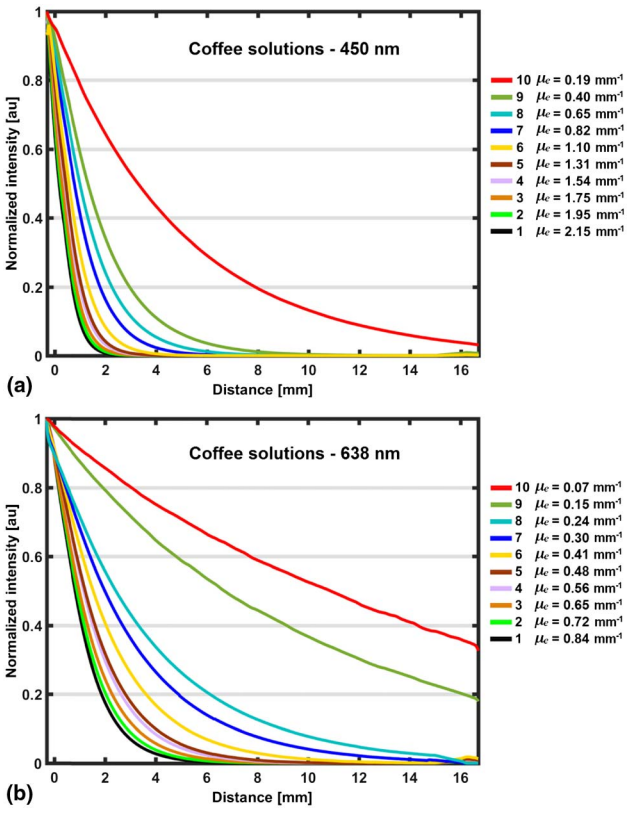

Fig. 11. Curves obtained by vertically integrating the SLIPI image results of the coffee solutions for 450 nm illumination wavelength in (a) and 638 nm in (b). The exponential decay of the light intensity as a function of distance through the cuvette is obtained here, and the extinction coefficient has been deduced from those decays.

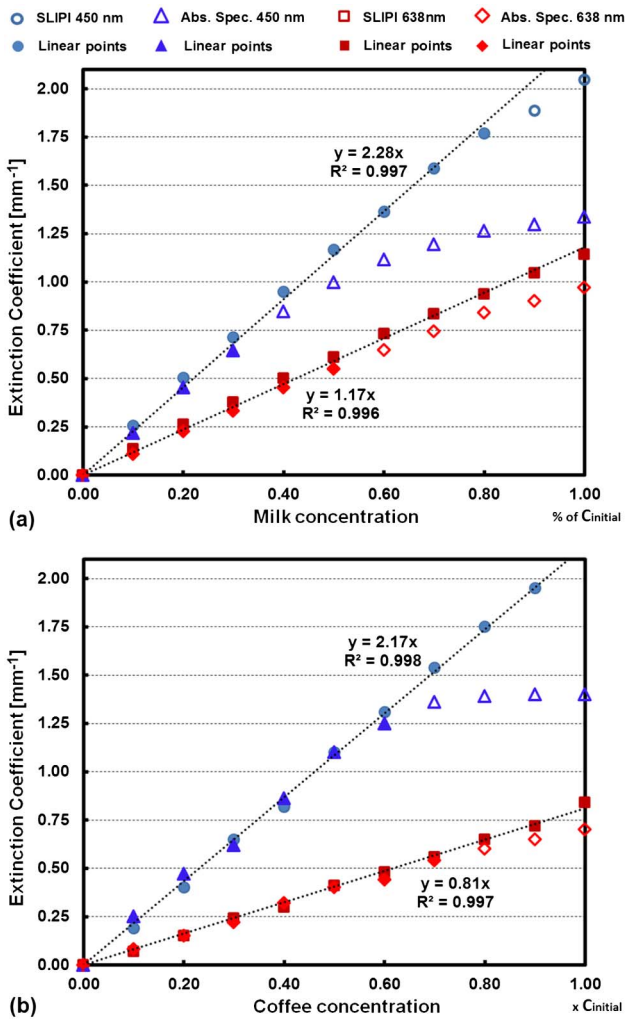

Fig. 12. Extinction coefficient results as a function of concentration for (a) milk and (b) coffee solutions. The SLIPI results show good linearity, while the absorption measurements show loose linearity.

Those curves have been plotted for all milk solutions in Fig. 10. It is seen that the curves decay more strongly as concentration increases, as expected. In addition, for a given concentration, the light extinction is more pronounced at 450 nm [Fig. 10(a)] than at 638 nm [Fig. 10(b)] illumination wavelength. This observation is in accordance with the results from absorption spectroscopy given Fig. 6. The SLIPI decay curves for the coffee solutions are shown in Fig. 11, where similar observations for the milk solution can be drawn. By now finding the best exponential fit for each of those curves, the extinction coefficient is extracted (as explained in Section 3.A) and displayed in the legends located on the right-hand of each graph. An analysis and comparison of those extinction coefficient results is given in the next section.

5. RESULTS COMPARISON

The results of extinction coefficient measurements obtained by absorption spectroscopy and SLIPI are given in this section for all prepared milk and coffee solutions. Figure 12(a) shows the results of the extinction coefficient as a function concentration for the case of the scattering milk solutions. Several observations can be made.

– The linearity between the extinction coefficient and the concentration is respected for both 450 nm and 638 nm illumination wavelengths at the extinction coefficient of $\mu_e < 0.60$ mm^{-1}. In this case, the measured values are found to be very similar between SLIPI and absorption spectroscopy measurements.

– The extinction coefficients are larger at 450 nm illumination than for 638 nm illumination for both SLIPI and absorption spectroscopy measurements.

– When $\mu_e > 0.60$ mm^{-1}, the linearity is lost for the absorption spectroscopy, which gives an underestimated value of the extinction coefficient. The more concentrated the solution, the larger the deviation between the measured value and its linear trend. This is explained by the increase of unwanted scattered and multiply scattered light detected when concentration increases.

– When $\mu_e > 0.60$ mm^{-1}, the linearity is preserved with the SLIPI measurements. However, at high milk concentration and for 450 nm illumination when $\mu_e > 1.80$ mm^{-1}, it is seen that the SLIPI results also lose linearity due to too low of a signal-to-noise ratio.

– The length of the cuvette used for absorption measurements is 4 mm. Thus, when $\mu_e = 0.60$ mm^{-1}, the optical

depth is OD = 2.4, which does not correspond to the single scattering regime anymore. Despite the spatial Fourier filtering optical configuration of the absorption setup, the system is not capable of rejecting all scattered light, explaining the underestimation of the extinction coefficient. On the contrary, SLIPI efficiently removes the contribution from multiple scattering, which allows more reliable measurements in turbid situations.

Figure 12(b) shows the results for the case of the absorbing coffee solutions. From those results, several observations can be made.

– For the absorption spectroscopy measurements at 450 nm, the linearity is well preserved for $\mu_e < 1.20$ mm^{-1}. Above this value, the extinction coefficient reaches a plateau as the transmitted optical signal falls below the detection limit of the instrument, as previously shown in Fig. 7(b). Thus, absorption is largely dominant over scattering, when exciting the coffee molecules at 450 nm, making the instrument performing well until its detection limit.

– For the absorption spectroscopy measurements at 638 nm, the linearity is once again lost when $\mu_e = 0.60$ mm^{-1}, in a similar fashion to that for the milk solutions. This effect demonstrates that scattering now plays a nonnegligible role in the extinction of light, explaining the "reddish" color of coffee observed from the photographs from Fig. 6.

– The SLIPI results of coffee show a very good linearity of the extinction coefficient with concentration, both for 450 nm and 638 nm illumination.

From the presented results, one can now divide the extinction coefficients at the two wavelengths such that $R = \mu_{e(450\,\mathrm{nm})}/\mu_{e(638\,\mathrm{nm})}$. As the concentration is identical for a given solution, R corresponds to the ratio of the extinction cross sections $(\sigma_{e(450\,\mathrm{nm})}/\sigma_{e(638\,\mathrm{nm})})$. This ratio is, therefore, an optical constant characterizing the probed liquid. Thus, reliable measurements should provide an identical ratio, independent of concentration. This is, in effect, obtained with the SLIPI measurements, as shown in Fig. 13, where $R_{\mathrm{milk}} = 1.9 \pm 0.019$ and $R_{\mathrm{coffee}} = 2.7 \pm 0.026$. Such results are not obtained with the absorption spectroscopy measurements where variable ratios are extracted.

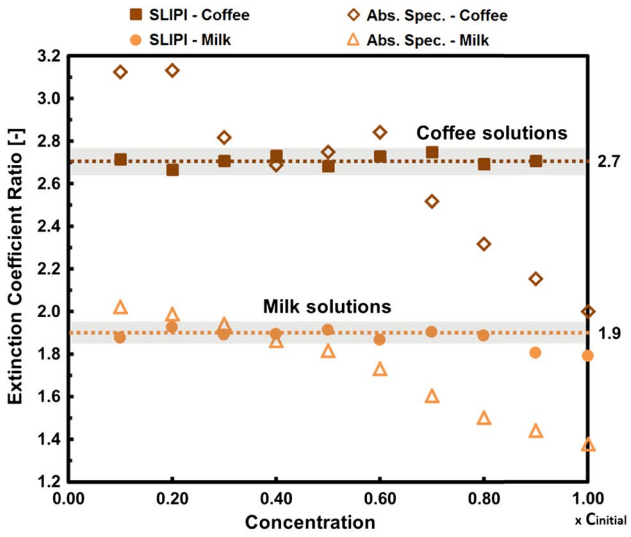

Fig. 13. Ratio of the extinction coefficients, $R = \mu_{e(450\,\mathrm{nm})}/\mu_{e(638\,\mathrm{nm})}$, as a function of concentration. The SLIPI results show, as expected, a constant ratio for both milk and coffee, where $R_{\mathrm{milk}} = 1.9$ and $R_{\mathrm{coffee}} = 2.7$.

6. CONCLUSIONS

SLIPI is capable of measuring the correct extinction coefficient in turbid solutions, where commercial absorption spectrometers fail. In the current study, reliable SLIPI measurements in scattering milk solutions could be obtained up to $\mu_e = 1.80$ mm^{-1}. This limit increases in the situation of absorbing liquids such as coffee. One way of extending the capability of the SLIPI measurement consists in reducing the field of view of the camera. In the present investigation, the camera was imaging over a distance of ~16 mm. If one would image over ~4 mm distance only, the technique would, due to the nondimensionless nature of the process, measure an extinction coefficient four times as high (above 7 mm^{-1}). Future work will focus on further developing the technique for measuring not only the extinction coefficient but also the scattering and absorption coefficients, respectively. Finally, another improvement would consist of illuminating the sample with a broadband light source as well as in detecting fluorescence for more specific characterization [22]. Based on the results of this study, it is believed that the SLIPI technique will replace, in the near future, the commonly used transmission approach for scattering solutions characterization.

Funding. H2020 European Research Council (ERC) (638546).

Acknowledgment. The authors wish to thank the International Science Program (ISP) of Uppsala University for equipment and financial support as well as the Lund Laser Center (LLC).

REFERENCES

1. A. Bose, P. P. Dash, and M. K. Sahoo, "Simple spectrophotometric methods for estimation of aceclofenac from bulk and formulations," Pharm. Methods **1**, 57–60 (2010).
2. T. Kruatian and K. Jitmanee, "Simple spectrophotometric method for determination of iodine value of vegetable oils," Chiang Mei J. Sci. **3**, 419–426 (2013).
3. C. M. Mullins, *Cardiac Catheterization in Congenital Heart Disease: Pediatric and Adult* (Blackwell Futura, 2006), pp. 296–297.
4. H. Ramachandran and A. Narayanan, "Two-dimensional imaging through turbid media using a continuous wave light source," Opt. Commun. **154**, 255–260 (1998).
5. S. Mujumdar and H. Ramachandran, "Imaging through turbid media using polarization modulation: dependence on scattering anisotropy," Opt. Commun. **241**, 1–9 (2004).
6. C. L. Wang, P. P. Ho, X. Liang, H. Dai, and R. R. Alfano, "Kerr–Fourier imaging of hidden objects in thick turbid media," Opt. Lett. **18**, 241–243 (1993).
7. E. Kristensson, E. Berrocal, and M. Aldén, "Quantitative 3D imaging of scattering media using structured illumination and computed tomography," Opt. Express **20**, 14437 (2012).
8. E. Berrocal, S.-G. Pettersson, and E. Kristensson, "High-contrast imaging through scattering media using structured illumination and Fourier filtering," Opt. Lett. **41**, 5612–5615 (2016).
9. F. Bevilacqua, A. J. Berger, A. E. Cerussi, D. Jakubowski, and B. J. Tromberg, "Broadband absorption spectroscopy in turbid media by

combined frequency-domain and steady-state methods," Appl. Opt. **39**, 6498–6507 (2000).
10. F. Foschum and A. Kienle, "Broadband absorption spectroscopy of turbid media using a dual step steady-state method," J. Biomed. Opt. **17**, 037009 (2012).
11. E. Berrocal, E. Kristensson, M. Richter, M. Linne, and M. Aldén, "Application of structured illumination for multiple scattering suppression in planar laser imaging of dense sprays," Opt. Express **16**, 17870 (2008).
12. E. Kristensson, L. Araneo, E. Berrocal, J. Manin, M. Richter, M. Aldén, and M. Linne, "Analysis of multiple scattering suppression using structured laser illumination planar imaging in scattering and fluorescing media," Opt. Express **19**, 13647 (2011).
13. Y. N. Mishra, F. Abou Nada, S. Polster, E. Kristensson, and E. Berrocal, "Thermometry in aqueous solutions and sprays using two-color LIF and structured illumination," Opt. Express **24**, 4949–4963 (2016).
14. E. Kristensson, E. Berrocal, and M. Aldén, "Two-pulse structured illumination imaging," Opt. Lett. **39**, 2584–2587 (2014).
15. E. Berrocal, J. Johnsson, E. Kristensson, and M. Aldén, "Single scattering detection in turbid media using single-phase structured illumination filtering," J. Eur. Opt. Soc. **7**, 12015 (2012).
16. E. Kristensson, J. Bood, M. Aldén, E. Nordström, J. Zhu, S. Huldt, P.-E. Bengtsson, H. Nilsson, E. Berrocal, and A. Ehn, "Stray light suppression in spectroscopy using periodic shadowing," Opt. Express **22**, 7711–7721 (2014).
17. E. Berrocal, D. L. Sedarsky, M. E. Paciaroni, I. V. Meglinski, and M. A. Linne, "Laser light scattering in turbid media. Part I: experimental and simulated results for the spatial intensity distribution," Opt. Express **15**, 10649 (2007).
18. M. L. Meade, "Advances in lock-in amplifiers," J. Phys. E **15**, 395–403 (1982).
19. H. F. Talbot, "Facts relating to optical science. No. IV," Philos. Mag. **9** (56), 401–407 (1836).
20. O. Ménard, S. Ahmad, F. Rousseau, V. Briard-Bion, F. Gaucheron, and C. Lopez, "Buffalo vs. cow milk fat globules: size distribution, zeta-potential, compositions in total fatty acids and in polar lipids from the milk fat globule membrane," Food Chem. **120**, 544–551 (2010).
21. K. M. Yoo, F. Liu, and R. R. Alfano, "Imaging through a scattering wall using absorption," Opt. Lett. **16**, 1068–1070 (1991).
22. W. Xu, T.-H. Kim, D. Zhai, J. C. Er, L. Zhang, A. A. Kale, B. K. Agrawalla, Y.-K. Cho, and Y.-T. Chang, "Make caffeine visible: a fluorescent caffeine "traffic light" detector," Sci. Rep. **3**, 2255 (2013).